Journal Name

ARTICLE

Real-time dynamic SERS detection of galectin using glycan-decorated gold nanoparticles

Received 00th January 20xx,
Accepted 00th January 20xx

DOI: 10.1039/x0xx00000x

www.rsc.org/

Judith Langer,[a,b] Isabel García[a,b] and Luis M. Liz-Marzán[a,b,c]

We present the application of surface-enhanced Raman scattering (SERS) spectroscopy for the fast, sensitive and higly specific detection of the galectin-9 (Gal-9) protein in binding buffer (mimicking natural condtions). The method involves the use of specifically designed nanotags comprising glycan-decorated gold nanoparticles encoded with 4-mercaptobenzoic acid. At fast time scales Gal-9 can be detected down to 1.2 nM concentration by monitoring the SERS signal of the reporter, driven by aggregation of the functionalized Au NPs tags, induced by Gal-9 recognition. We additionally demonstrate that the, sensitivity and concentration work range of the sensor can be tuned via control of aggregation dynamics and cluster size distribution.

Introduction

Galectins are a family of conserved carbohydrate-binding proteins, characterized by their affinity toward β-galactoside residues.[1] They are involved extracellularly in interactions with cell-surface and matrix glycoproteins and glycopeptides, whereas intracellularly they interact with nuclear and cytoplasmic proteins that initiate signaling processes. It is also well-known that galectins play major roles in cancer[2] (apoptosis, metastasis and angiogenesis) and in immune processes[3] (inflammatory response, pathogen recognition). In addition, alterations in galectin expression have been reported in experimental models and also in cancer patients, and as a result galectin profiles may be considered as biomarkers of disease evolution.[4,5,6]

Many of these biological functions are possible due to the multivalent carbohydrate-lectin binding, where galectins act as cross-interaction targets. Therefore, the interest in detecting and quantifying various galectins present in patient fluids for diagnosis and prognosis has largely increased in recent years. Most of the proposed detection methods are based on enzyme-linked immunosorbent assays (ELISA) and/or Western blot analysis,[7,8,9] both methods relying on the availability of galectin-specific antibodies. As noted above, the topology of the multivalent interaction mediated by galectins is assumed to be crucial for signaling purposes. In this context, there is a need to have alternative and convenient analytical methods, based on selective galectin labeling substrates or chemical probes that provide information regarding the multivalency stage of galectins.

Microarray-based detection assays for the galectin family, which make use of antibodies immobilized on porous aluminum matrices, have been described as alternative approaches to proteomic tools.[10] Detection and binding partners of diverse galectins have been investigated and identified using carbohydrate microarrays.[11,12] However, only few alternative techniques based on chemical-linked probes have been developed for sensing galectin cancer biomarkers.[13,14]

Surface enhanced Raman scattering (SERS) has emerged as one of the most powerful and sensitive analytical tools, with extremely low detection limits down to the single-molecule level,[15] which has opened up multiple applications in biosensing. Targets such as aminoacids,[16] different DNA bases and sequences, [17,18,19,20,21,22,23] small proteins[24] as well as complex proteins[25,26] (serum albumin, enzymes, etc.) and even cells or cell compartments,[27,28,29] have been intensively investigated. However, the SERS spectroscopy of complex biological matter often suffers from serious limitations. The interaction between nanoparticles and proteins, as well as the random orientation of the latter, typically lead to broadening of vibrational fingerprint peaks. Additionally, the often extremely low Raman cross section of proteins, combined with low densities (e.g. bulky proteins), makes direct biomolecular detection highly challenging. To overcome such limitations, an indirect sensing method based on using SERS probes can be applied, which typically involves a plasmonic core nanoparticle as optical enhancer, covered with a self-assembled monolayer of Raman reporter molecules with

[a] CIC biomaGUNE, Paseo de Miramón 182, 20014 Donostia-San Sebastián, Spain.
[b] Biomedical Research Networking Centre on Bioengineering, Biomaterials and Nanomedicine (CIBER-BBN), Paseo Miramón 182 , 20014 Donostia-San Sebastián, Spain
[c] Ikerbasque, Basque Foundation for Science, 48013 Bilbao, Spain.

Electronic Supplementary Information (ESI) available: additional characterization of SERS nanotags and time-resolved SERS detection studies. See DOI: 10.1039/x0xx00000x

high SERS cross section as the label. The implementation of molecular recognition moieties toward a specific biomarker can be used to target the component of interest, and the complete ensemble is known as SERS nanotag.[30] Indirect biosensing platforms using SERS nanotags can also work when successful recognition events cause changes in the SERS reporter signal. This indirect sensing strategy has been recently applied using carbohydrate-coated silver nanoparticles, mimicking the monosialotetrahexosylganglioside (GM1) surface, and have been proposed for the selective detection of cholera toxin B subunit (CTB), using SERS.[31] We present the use of SERS toward the detection of human, tandem type galectins, exploiting the selective affinity of these proteins toward β-galactoside residues. The proposed platform comprises gold nanoparticles (Au NPs) decorated with glycans and with the Raman reporter 4-mercaptobenzoic acid (4-MBA) to sensitize the SERS signal. Our solution-based method relies on the SERS read-out of Au NP aggregation, induced by the specific molecular recognition of galectin by the galactose head groups of the ligand. As galectins appear in different structures and valence states such as monomer (monovalent), dimer, tandem (divalent) or chimera (multivalent), the aggregation-based sensing strategy principally discriminates between monovalent (no aggregation) and di- or multivalent galectins (aggregation). For our proof-of-concept study human galectin-9 (Gal-9), belonging to the type of tandem-repeated galectins, was selected as protein detection model. Gal-9 contains two carbohydrate recognition domains (CRDs) within a single polypeptide chain, separated by a peptide linker.[32] This galectin is expressed by a variety of tumour cells and plays an important role in tumour immunity.[33]

NP aggregation is a dynamic process driven by the concentration of reactants (here SERS nanotag and Gal-9) which needs to be understood (and controlled) prior to building a reliable, aggregation-based SERS sensor. To this aim, the time-dependent SERS response was investigated as function of Gal-9 concentration. It should be noted that, the presence of further components within the sample can affect reactant diffusion, reactivity, aggregation speed/state and ultimately the measured SERS signal. To mimic a more realistic sample (e.g. serum), we studied also the possible interference of a non-binding protein on the Gal-9 association behaviour, using different ratios of Gal-9 and human serum albumin (HSA) mixtures.

Results and Discussion

Design of the SERS sensor

The design of the SERS detection strategy is schematically illustrated in **Fig. 1**. The sensor comprises 30 nm (spherical) Au NPs labeled with the Raman reporter 4-MBA for detection and with specific glycans for targeting. The electromagnetic field enhancement at the Au NPs surface due the excitation of localized surface plasmon resonances (LSPRs) is relatively low for isolated spherical nanoparticles, as compared to other anisotropic morphologies. As a consequence, the SERS enhancement factor, defined as the ratio between SERS and Raman signals under the same measurement conditions, even for SERS reporter molecules with high Raman cross sections, is therefore small and often lies below the detection limit for isolated Au NPs in solution.[34] The situation changes dramatically when these nanoparticles are in close contact. The reduced inter-particle distance gives rise to coupling between the individual LSPR modes into new LSPR modes. Such hybridized modes are characterized by extremely high electromagnetic fields confined within the junctions between nanoparticles, usually termed hotspots. Molecules located within hotspots are thus exposed to largely enhanced fields and therefore display much stronger Raman scattering, ultimately leading to enhancement factors of up to 10^8.[35,36] Plasmon coupling and hotspot formation are behind the basic idea of our sensing strategy. The prepared SERS nanotags do not provide a readable Raman scattering signal when spatially well separated (large enough interparticle distances), but a clear signal from the SERS reporter can be detected once aggregation is initiated, upon selective targeting of Gal-9 by the surface glycans (**Fig. 1**). The SERS signal intensity thereby correlates with the aggregation state of the nanotags, which reflects the cluster size distribution. As aggregation is a dynamic process, the SERS signal intensity becomes time-dependent, thereby providing information on the cluster growth progress.

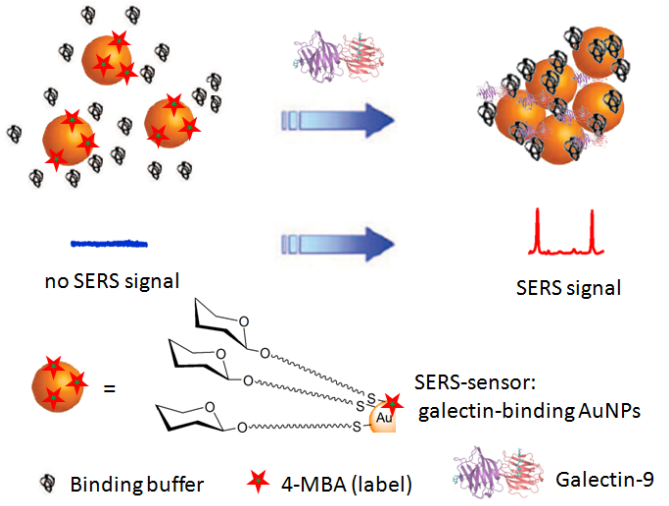

Fig. 1 Sensing strategy toward detection of Gal-9 through molecular recognition-based aggregation of Au NP SERS nanotags.

Preparation and characterization of SERS nanotags

Conjugation of stabilizing molecules onto the surface of the Au NPs was found to be essential toward proper function of the SERS nanotags. Previously reported work in our group described the use of low molecular weight neoglycoconjugates with amphiphilic character, to provide anisotropic Au NPs with high colloidal stability in protein-rich physiological media.[37] The amphiphilic nature of the linker used to immobilize the carbohydrates is crucial toward providing long-term stability against aggregation. Additionally, a carbohydrate-coating confers biocompatibility and targeting specificity to their natural receptors, i.e. carbohydrate-binding proteins.[37] We selected 4-MBA as the Raman reporter molecule

because of its high photochemical stability, the presence of a thiol group with high affinity to Au NP surfaces[38] and the deprotonated state of the acidic function under physiological conditions, which additionally avoids self-aggregation by inducing repulsive charge-charge interactions.

SERS nanotags were prepared by simultaneous binding of a thiol-containing lactose glycoconjugate[37] and the 4-MBA Raman reporter, as adapted from Porter et al.[39] Specificity, assay sensitivity and dynamic range depend on various parameters, including nanoparticle size and Raman reporter/ligand density.[40] We therefore tested different Au NP sizes (30, 42, 60 nm) and reporter/glycan ratios, so as to identify the most effective SERS nanotag configuration, by comparing the UV-vis and SERS spectra in the absence and in the presence of Gal-9. As expected, we found a clear correlation between particle size and colloidal stability. Larger particles were less resistant against aggregation (for constant ratios between reporter/glycan and available NP surface). We ultimately selected Au NPs with an average diameter of 30 nm, and the reporter/glycan ratio was then further optimized for stabilization against coalescence under the required physiological binding conditions, while providing a high density of binding sites for Gal-9 and maximum SERS reporter signal. Citrate-stabilized Au NPs ([Au] = 0.4 mM) were thus functionalized in water by ligand exchange, using the corresponding lactose glycoconjugate (1.05 µM) and 4-MBA (210 nM) solutions, in a molar ratio of 5:1 (see details in the Experimental section). The SERS nanotags were characterized by UV-Vis spectroscopy, transmission electron microcopy (TEM) and ^{1}H-NMR spectroscopy. **Fig. 2A** shows the UV-Vis spectra of Au NPs before (citrate-Au NPs) and after incubation with a mixture of lactose glycoconjugate and 4-MBA. SERS nanotags display a single absorbance band at 530 nm (**Fig. 2A**), with no significant broadening as compared to the original colloid. The corresponding TEM images show high monodispersity and an average diameter of 30 nm (**Fig. 2B** and **Fig. S1** in SI). Successful conjugation of lactose glycoconjugate and 4-MBA was verified using ^{1}H-NMR spectroscopy (**Fig. S2** in SI).

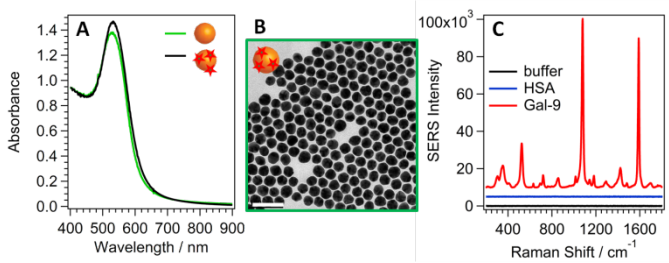

Fig. 2 (A) UV-vis spectra of citrate-stabilized Au NP colloids (green) and after binding of lactose glycoconjugate and 4-MBA (black). (B) Representative TEM micrograph of functionalized SERS nanotags. The white scale bar corresponds to 100 nm. (C) SERS spectra of the nanotags upon incubation with 15 µL pure buffer solution (black), Gal-9/binding buffer solution (red) and non-binding HSA/binding buffer solution (blue).

Sensing Gal-9

The as-prepared SERS nanotags decorated with specific galectin-interacting glycan and 4-MBA did not yield any SERS signal, even upon incubation with pure buffer (black curve in **Fig.** 2C). In contrast, an intense signal coinciding with the SERS fingerprint of 4-MBA, including the characteristic C-C ring stretch vibrations at 1078 and 1585 cm^{-1}, was recorded in the assay of 2 nM Gal-9 (red curve in **Fig. 2C**). A control experiment was carried out to verify the specificity of the galectin-responsive SERS nanotags. Upon addition of a different protein, such as human serum albumin (HSA), to the SERS nanotag solution, no SERS signal was obtained (blue curve in **Fig. 2C**), clearly indicating the high specificity associated to the Gal-mediated assembly. Further, the specificity of the sensor was also tested with other galactose-binding proteins. Human galectin-1 (Gal-1), a prototypical monomeric protein (at concentrations below 80 nM)[41,42], and the legume *erythrina cristagalli lectin* (ECL), a non-galectin dimer, were selected as controls. Incubating the SERS nanotags with Gal-1 did not cause aggregation and thus the absence of SERS signal indicated a positive discrimination of the sensor against monomer galectins. The addition of ECL to the functionalized Au NPs did not result in appreciable SERS intensity either, supporting the sensor selectivity toward tandem-repeated type galectins.

The limit of detection (LOD) was investigated using the optimized SERS tags with different Gal-9 concentrations. 300 µL of glycan-Au NP SERS nanotag solution (3.6×10^{12} NP/mL) was mixed with 15 µL aliquots of different Gal-9 concentrations in binding buffer (mixing ratio 20:1), resulting in final Gal-9 concentrations between 0.4 and 2 nM (**Fig. S3** in SI). Incubation of SERS nanotags with the highest Gal-9 concentration led to immediate aggregation, visible by instantaneous colour change from red to purple. In contrast, for low concentrations down to 1.2 nM no colour change was appreciated, whereas the SERS signal was readily detectable. At lower concentrations, a significant induction time was required prior to detection of a meaningful SERS signal. By increasing the incubation time to 12 h the LOD could be improved down to 0.8 nM. This indicates that both Au NP cluster size and aggregation dynamics are strongly dependent on the concentration of Gal-9. In order to determine the optimal dynamic range of our SERS sensor, time-resolved SERS measurements over time scales ranging from minutes to several hours were performed for different Gal-9 concentrations between 2 and 1.2 nM (corresponding to 5 and 3 Gal-9 proteins per SERS nanotag, respectively). The intensity of the peak at 1078 cm^{-1} was plotted as a function of time (**Fig. S3** in SI). The Gal-9-induced SERS signal profile in the range 2 – 1.6 nM displayed a similar behaviour to the earlier reported kinetics for Ag NP aggregation induced by formation of triplex DNA strands[43] or for the aggregation of Au and Ag NPs, in the presence of mercaptobenzimidazol, mediated by different electrolytes.[44] The recorded profile can be interpreted as follows: fast Au NP aggregation within the first 30 s is reflected by a steep and linear SERS signal increase, whereas slower growth into bigger clusters within the following 2 minutes is indicated by a slower asymptotic increase, until the signal starts to slightly decrease, which can be related to detuning between excitation laser and LSPR wavelengths, due to large LSPR redshifts with increasing cluster sizes. The profile changed for Gal-9 concentrations below 1.6 nM, in which a continuously rising SERS intensity indicates a slow Au NP aggregation.

Unfortunately, the dynamic SERS profiles recorded from the assays at 2 and 1.8 nM Gal-9 concentration were not sufficiently reproducible. In some cases, the steep intensity increase was

followed by a fast decrease within the first minute or by the occurrence of larger signal fluctuations, leading to poor reliability of the data. These effects can be explained by the observed precipitation of large clusters during the fast, uncontrolled growth. The results indicate that a key issue toward improving performance and concentration range of the Gal-9 SERS sensor is the control of nanoparticles aggregation. This is in agreement with a related study, in which Darby and LeRu reported that the injection of a small volume of a concentrated analyte solution into a nanoparticle colloid can induce fast nanoparticle aggregation events, which are extremely difficult to control, leading to non-reproducible SERS signals.[45] This problem was solved by using a balanced mixing volume ratio for both components, so as to provide a more homogeneous distribution of both reactants and to avoid high concentration gradients within the interaction volume. This approach was applied to our sensor by using a mixing volume ratio of 150 µL:150 µL (mixing ratio 1:1) and adjusting the concentration of the SERS nanotag (2× more concentrated), so as to reach the same final Au NP concentration as in the above described measurements.

Time-dependent SERS experiments were thus performed to monitor the aggregation dynamics, for Gal-9 concentrations between 4 and 1.2 nM (**Fig. 3**). The SERS signal was observed immediately after incubation, down to 1.6 nM, which thus corresponds to the LOD. This indicates that the aggregation is still fast enough to be detectable in a real-time configuration, whereas dilution of the initial concentrations of protein and SERS nanotag results in a significant decrease of the aggregation rate. As a consequence, aggregation became more controllable but the LOD was twice as high and the SERS intensities obtained for the same Gal-9 final concentrations were lower. Here, the time-dependent SERS signal profiles (4 – 3.2 nM) also revealed three steps with different dynamics: (1) a fast aggregation with linear SERS response in the early time window, followed by (2) a slower aggregation process with non-linear SERS signal increase, to then (3) reach a plateau (equilibrium) without further SERS intensity changes. Interestingly, the durations of the linear stage, the rise and the plateau were found to depend on the concentration of Gal-9. At lower concentrations the duration of the linear stage increased, while the steepness (**Fig. S4**) and intensity at the plateau (**Fig. 3A**) were lower, indicating a slower aggregation and formation of smaller clusters when lowering the concentration of Gal-9. At 2.4 nM concentration, the aggregation kinetics were too slow and no plateau could be reached, whereas for 1.6 nM the signal did not vary within the observation time window (**Fig. 3A**).

The working range of the SERS sensor can be illustrated by plotting the SERS intensity of the 1078 cm^{-1} vibration as a function of Gal-9 concentration. These values were extracted from time-dependent data sets using spectra collected at t = 200 s and then linearly fitted (**Fig. 3B**). The plot indicates that the SERS nanotag concentration determines the working range of the sensor. At lower SERS nanotag concentration (20:1 mixing volume ratio) a lower detection limit was reached but the working range was only half of that obtained when using a twice as high nanotag concentration (1:1 mixing volume ratio). This suggests that SERS nanotag concentration and working range are linearly correlated. The dynamic range obtained here (**Fig.3B**) is relatively small but fits within the range required for detection of enhanced Gal-9 concentration from patients with infections of dengue virus or with an inflammatory disease.[46,47]

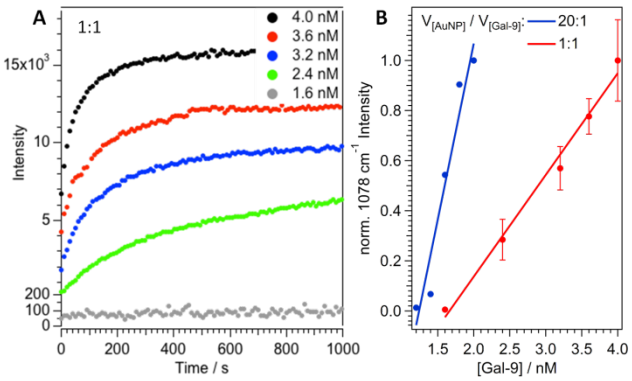

Fig. 3 (A) Time-dependent evolution of the SERS intensity at 1078 cm^{-1}, for different Gal-9 concentrations in the 1:1 volume mixing ratio configuration. (B) Normalized concentration-dependent SERS intensities for Au NP/Gal-9 volume mixing ratios of 20:1 and 1:1.

To gain more detailed insight on the aggregation process, 3.6 nM (high concentration range) and 1.6 nM (low concentration range), in the 1:1 mixing configuration were also studied by complementary optical methods. Dramatic changes in the UV-vis spectra of the glycan-SERS nanotags were observed over time upon mixing the nanoparticles with 3.6 nM Gal-9 (**Fig. 4A,B**). The LSPR at 530 nm originating from isolated Au NPs rapidly decreases in intensity as a new plasmon band develops at 730 nm, arising from a coupled LSPR mode, due to aggregation of the nanoparticles. In contrast, such changes were not observed when the Gal-9 concentration was as low as 1.6 nM (**Fig. 4C**). However, our previous SERS experiments (**Fig. 3**) showed that such a low concentration of Gal-9 can be detected in our approach, indicating that partial aggregation of the SERS nanotags must occur. A kinetic study by dynamic light scattering (DLS) confirmed a fast and continuously increasing hydrodynamic diameter up to 750 nm in the 3.6 nM Gal-9 assay leading to large cluster sizes, whereas the 1.6 nM Gal-9 assay only showed an increase of 40 nm relative to the 45 nm value measured for nanoparticles in pure buffer solution without Gal-9, as control. The hydrodynamic diameter of the control did not vary within the time window of 16 minutes, confirming the stability of the SERS nanotags in the presence of the binding buffer. The 40 nm increase indicates that the protein recognition process for the low concentration results in the formation of Au NP dimers, but not in larger clusters. TEM images obtained from the samples after the DLS study provided additional evidence that the SERS nanotags were well-dispersed, with a small degree of NP dimerization in the case of low Gal-9 concentration, while large µm-sized aggregates were formed in the presence of 3.6 nM Gal-9 (**Fig. 4D, E**). These findings clearly confirm the Gal-9-controlled aggregation observed in the SERS experiments (**Fig. 3**). We thus conclude that, the aggregation process is triggered by specific Gal-9 recognition events, rather than non-specific interactions or salt-induced aggregation.

The NP dimerization was analysed in more detail and could be quantified as ca. 4% by counting monomers and dimers from a larger TEM area containing over 400 NPs. This small amount of NP

dimers is sufficient to generates a meaningful SERS signal, whereas the UV-vis extinction measurement under the same conditions is not sensitive enough, again supporting the high sensitivity of the SERS method.

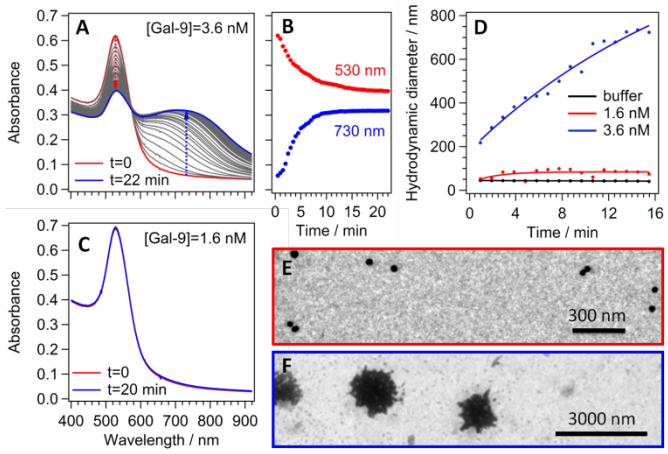

Fig. 4 (A) Time-dependent UV-vis spectra of SERS nanotags incubated with Gal-9 at a concentration of 3.6 nM. The red curve corresponds to the SERS nanotags right after addition of Gal-9, where aggregation did not start (t=0); the blue curve corresponds to highly aggregated Au NPs (t=22 min). (B) Plot of the extinction intensity at 520 nm (red) and 730 nm (blue), as indicated by red and blue arrows in A, respectively, as a function of time. (C) UV-vis spectra of SERS nanotags incubated with Gal-9 at a final concentration of 1.6 nM, at both t=0 (red) and t=20 min (blue). (D) Average particle diameter obtained from DLS versus time under the same conditions as the UV-vis spectra. Gal-9 concentrations are indicated in the graph. (E,F) TEM images of SERS nanotags after incubation assays with 1.6 nM (E) and with 3.6 nM Gal-9 (F).

To mimic a more realistic environment for our Gal-9 sensing approach, the SERS response was also probed for mixtures of specifically and non-specifically binding proteins. Therefore, Gal-9/HSA mixtures with ratios of 4:1, 3:2 and 2:3, corresponding to 1.6, 1.2 and 0.8 nM final Gal-9 concentrations (total protein concentration = 2 nM), were incubated with SERS nanotags (according to the 20:1 mixing volume ratio procedure). In this case, the SERS intensities were much lower than those from the corresponding samples incubated with pure Gal-9 and the LOD level increased to 1.6 nM, indicating a significant stabilizing effect of the HSA protein against Au NP aggregation. The dynamic SERS profiles clearly support that the presence of HSA reduced significantly the aggregation rate and the SERS signal intensity, thus indicating hindered aggregation and formation of smaller clusters (**Fig. S5** in SI). When using a fixed Gal-9 concentration of 1.6 nM and successively increasing the amount of HSA in Gal-9/HSA mixtures with ratios of 4:1, 2:1, 4:3 and 1:1, the SERS intensity followed the same trend: with increasing HSA concentration Gal-9 recognition was slowed down, leading to smaller aggregates (**Fig. S5** in SI).

Experimental

Materials

Deionized water from a Millipore Milli-Q system (resistivity >18 MΩ·cm) was used in all experiments. Hydrogen tetrachloroaurate trihydrate ($HAuCl_4 \cdot 3H_2O$), sodium borohydride, ascorbic acid, silver nitrate, sodium chloride (NaCl), potassium chloride (KCl), magnesium chloride hexahydrate ($MgCl_2 \cdot 6H_2O$), calcium chloride dihydrate ($CaCl_2 \cdot 2H_2O$), sodium dodecylsulfate (SDS), hydrochloric acid (HCl), human serum albumin (HSA) and 4-mercaptobenzoic acid (4-MBA) were purchased from Sigma. The β-galactoside-binding lectin galectin-9 (Gal-9) was purchased from Abcam. Dialysis membranes with a molecular weight cut-off (MWCO) of 100 kDa (cellulose ester) and ultrafiltration membranes (regenerated cellulose) were purchased from Millipore. The neoglycoconjugate of galatose β-D-galactopyranosyl-(1–4)-D-glucose (Lac) was synthesized as previously described.[48]

Methods

Transmission electron microscopy (TEM) images were obtained in a field-emission high-resolution Philips JEOL JEM-2100F electron microscope, at an acceleration voltage of 200 kV. Samples for TEM analysis were prepared by drop-casting the diluted solutions of SERS nanotags on holey carbon-coated Cu mesh grids (400 mesh) and air-dried at room temperature. SERS measurements were performed by means of an InVia Reflex Raman system (Renishaw) comprising a microscope (Leica), a 785 nm laser excitation source (nominal output 260 mW) and a spectrometer equipped with a 1200 grooves/mm diffraction grating and a front-illuminated Peltier-cooled CCD detector (1024 pixels × 512 pixels). Dynamic light scattering (DLS) measurements were performed in a Malvern Zetasizer 3000 HS particle size analyzer (Malvern Instruments, UK). UV-vis absorption spectra were recorded at room temperature, using a Beckman Coulter DU 800 spectrometer.

Preparation of SERS nanotags

28 nm Au NPs were synthesized following a reported seeded growth protocol.[49] Au seeds (~ 10 nm, ~3×10^{12} NP/mL) were prepared by the standard citrate reduction method; a solution of sodium citrate (150 mL, 2.2 mM) was heated for 15 min under vigorous stirring until boiling, followed by injection of a solution of $HAuCl_4$ (1 mL, 25 mM). The colour of the solution changed from yellow to bluish grey and then to soft pink in 10 min. Immediately after the synthesis of the Au seeds the solution was cooled down to 90 ºC. Then, 1 mL of $HAuCl_4$ solution (25 mM) was injected. After 30 min the reaction was terminated and this process was repeated twice. The final concentration of metallic gold was 0.4 mM in the sample. For functionalization of Au NPs with the galactose-containing neoglycoconjugate and 4-MBA, an aqueous solution (210 µL) containing 100 molecules/nm^2 of lactose conjugate and methanolic solution (42 µL) containing 20 molecules /nm^2 of MBA were added dropwise simultaneously, under vigorous stirring, to as-synthesized Au NPs (1 mL, [Au] = 0.4 mM). The mixture was allowed to react for 2 h. SERS-active Au NPs were then filtered by using an Amicon Ultra centrifugal filter (100 000 MWCO, Millipore) at 18 ºC and 3000g, purified twice to remove excess carbohydrate and reporter and finally redispersed in 1 mL of water ([Au] = 0.4 mM).

Binding buffer

Gal-9 was reconstituted at a concentration of 0.5 mg/mL, in 20 mM Tris-HCl, 100 mM NaCl, pH=8 buffer and stored at 4 ºC. For Gal-9-mediated Au NPs assembly, the binding buffer was prepared by dilution of the stock Gal-9 solutions up to 5 mM NaCl.

Gal-9 molecular recognition SERS assay

In the SERS assay with Gal9 protein as the target, 15 µL of pure binding buffer (control), Gal-9 sample solution (final concentrations ranging from 0.8 to 2 nM in binding buffer) or HSA in binding buffer were added to 300 µL of SERS nanotags (~3.6×10^{12} NP/mL). The resulting mixture was immediately used for SERS measurements. The SERS spectra of the assays were recorded from solution, in glass vials (1 mL), exciting with a 785 nm laser focused through a 10× objective (numerical aperture = 0.25), using power of 16mW with integration time of 20s (static mode) or of 80mW with integration time of 1s for higher time resolution. The influence of the ratio of mixing volumes of Gal-9 protein target and SERS nanotags was evaluated using a similar procedure but changing the respective volumes of both components, i.e. 150 µL or 100 µL of Gal-9 solution in binding buffer were added to 150 µL or 200 µL of SERS nanotags. The aggregation and signal collection were performed according to the same protocol described above. Parameters for time-resolved measurements were used laser power of 80mW and 10s integration time (contineous scan).

Conclusions

By using glycan-decorated SERS nanotags we were able to detect Gal-9 in a selective and sensitive fashion, down to the nanomolar range. The detection limit was shown to depend on the volume mixing ratio between SERS nanotags and Gal-9 solution. Surface chemistry design in terms of targeting and stabilizing ligands versus Raman reporter densities is important for producing specific Gal-9 mediated aggregation of Au NPs. The SERS nanotags did not aggregate in the presence of pure binding buffer or non-specific protein HSA, and indicating that the aggregation is not a result of salt-induced nucleation or unspecific protein binding processes. The absence of the SERS signal in samples containing monovalent Gal-1 and divalent non-galectin ECL support the selectivity of the sensor toward tandem-repeated type galectins. The aggregation dynamics, and in turn the SERS response, strongly depend on the volume mixing ratios between SERS nanotags and Gal-9. A mixing ratio of 20:1 leads to extremely fast aggregation and to low data reproducibility. In contrast, a mixing ratio of 1:1 leads to a slower nucleation rate but controllable aggregation, lower SERS response and higher LOD but wider working range than in the 20:1 configuration. Finally, time-resolved measurements revealed that the aggregation process shows three different dynamic ranges, early, fast cluster growth, followed by slower aggregation before reaching the final equilibrium state. In general, the aggregation rate increases with rising Gal-9 concentration, thereby leading to larger clusters and higher SERS response. The great advantage of the SERS sensor is higher sensitivity, leading to a lower LOD compared to UV-vis detection. The work performance of the sensor is also affected by the presence of additional proteins in the solution. The non-specifically binding protein HSA protein was found to lower the Gal-9 recognition sensitivity, likely due to hindering of the fast diffusion of Gal-9 toward the glycan binding sites. This results in slower aggregation rates, smaller aggregates and lower SERS intensities. As the glycan molecules in the recognition probes can be easily replaced by other biologically relevant saccharides, the design can be conveniently adapted to the detection of other multivalent galectins or even to different biological targets.

Acknowledgements

We thank Dr. Christoph Hanske for TEM measurents. This work has been supported by the Spanish Ministerio de Economía y Competitividad MINECO (grant: MAT2013-46101-R).

Notes and references

1 H. J. Gabius, *Eur. J. Biochem.*, 1997, **243**, 543–576.

2 F.-T. Liu and G. A. Rabinovich, *Nat. Rev. Cancer*, 2005, **5**, 29–41.

3 G. a Rabinovich and M. a Toscano, *Nat. Rev. Immunol.*, 2009, **9**, 338–352.

4 J. He and L. G. Baum, *Lab. Invest.*, 2006, **86**, 578–90.

5 N. Hrynchyshyn, P. Jourdain, M. Desnos, B. Diebold and F. Funck, *Arch. Cardiovasc. Dis.*, 2013, **106**, 541–546.

6 V. Balan, P. Nangia-Makker and A. Raz, *Cancers (Basel).*, 2010, **2**, 592–610.

7 T. Fukumori, Y. Takenaka, N. Oka, T. Yoshii, V. Hogan, H. Inohara, H. O. Kanayama, H. R. C. Kim and A. Raz, *Cancer Res.*, 2004, **64**, 3376–3379.

8 I. Iurisci, N. Tinari, C. Natoli, D. Angelucci, E. Cianchetti and S. Iacobelli, *Clin. Cancer Res.*, 2000, **6**, 1389–1393.

9 J. Shen, M. D. Person, J. Zhu, J. L. Abbruzzese and D. Li, *Cancer Res.*, 2004, **64**, 9018–9026.

10 H. Van Hattum, N. I. Martin, R. Ruijtenbeek and R. J. Pieters, *Anal. Biochem.*, 2013, **434**, 99–104.

11 T. Horlacher, M. A. Oberli, D. B. Werz, L. Kröck, S. Bufali, R. Mishra, J. Sobek, K. Simons, M. Hirashima, T. Niki and P. H. Seeberger, *ChemBioChem*, 2010, **11**, 1563–1573.

12 X. Li, S. J. H. Martin, Z. S. Chinoy, L. Liu, B. Rittgers, R. A. Dluhy and G. J. Boons, *Chem. - A Eur. J.*, 2016, **22**, 11180–11185.

13 L. Ballell, M. van Scherpenzeel, K. Buchalova, R. M. Liskamp and R. J. Pieters, *Org Biomol Chem*, 2006, **4**, 4387–4394.

14 Y. K. Park, B. Bold, W. K. Lee, M. H. Jeon, K. H. An, S. Y. Jeong and Y. K. Shim, *Int. J. Mol. Sci.*, 2011, **12**, 2946–2957.

15 S.-R. Nie, S. and Emory, *Science.*, 1997, **275**, 1102–1106.

16 B. Fazio, C. D'Andrea, A. Foti, E. Messina, A. Irrera, M. G. Donato, V. Villari, N. Micali, O. M. Maragò and P. G. Gucciardi, *Sci. Rep.*, 2016, **6**, 26952.

17 K. Kneipp, H. Kneipp, V. Kartha, R. Manoharan, G. Deinum, I. Itzkan, R. Dasari and M. Feld, *Phys. Rev. E*, 1998, **57**, 6281–6284.

18 A. Barhoumi, D. Zhang, F. Tam and N. J. Halas, *J. Am. Chem. Soc.,* 2008, **130**, 5523–5529.

19 Y. C. Cao, R. Jin and C. a Mirkin, *Science.*, 2002, **297**, 1536–1540.

20 L. Barrett, J. a Dougan, K. Faulds and D. Graham, *Nanoscale*, 2011, **3**, 3221-3227.

21 M. M. Harper, J. a Dougan, N. C. Shand, D. Graham and K. Faulds, *Analyst*, 2012, **137**, 2063–2068.

22 L. Guerrini, Ž. Krpetić, D. Van Lierop, R. A. Alvarez-Puebla and D. Graham, *Angew. Chemie - Int. Ed.*, 2015, **54**, 1144–1148.

23 A. Torres-Nunez, K. Faulds, D. Graham, R. A. Alvarez-Puebla and L. Guerrini, *Analyst*, 2016, 5170–5180.

24 I. Pavel, E. McCarney, A. Elkhaled, A. Morrill, K. Plaxco and M. Moskovits, *J. Phys. Chem. C*, 2008, **112**, 4880–4883.

25 L. Xu, C. Zong, X. Zheng, P. Hu, J. Feng and B. Ren, *Anal. Chem.*, 2014, **86**, 2238–2245.

26 J. Lin, R. Chen, S. Feng, J. Pan, Y. Li, G. Chen, M. Cheng, Z. Huang, Y. Yu and H. Zeng, *Nanomedicine Nanotechnology, Biol. Med.*, 2011, **7**, 655–663.

27 L. a. Lane, X. Qian and S. Nie, *Chem. Rev.*, 2015, **115**, 10489–10529.

28 J. Taylor, a Huefner, L. Li, J. Wingfield and S. Mahajan, *Analyst*, 2016, **141**, 5037–5055.

29 M. Vendrell, K. K. Maiti, K. Dhaliwal and Y.-T. Chang, *Trends Biotechnol.*, 2013, **31**, 249–257.

30 Y. Wang and S. Schlücker, *Analyst*, 2013, **138**, 2224–2238.

31 J. Simpson, D. Craig, K. Faulds and D. Graham, *Nanoscale Horiz.*, 2016, **1**, 60–63.

32 M. Nagae, N. Nishi, T. Murata, T. Usui, T. Nakamura, S. Wakatsuki and R. Kato, *J. Biol. Chem.*, 2006, **281**, 35884–35893.

33 G. A. Rabinovich, F. T. Liu, M. Hirashima and A. Anderson, *Scand. J. Immunol.*, 2007, 66, 143–158.

34 Y. Zhang, B. Walkenfort, J. H. Yoon, S. Schlücker and W. Xie, *Phys. Chem. Chem. Phys.*, 2015, **17**, 21120–21126.

35 D. A. Genov, A. K. Sarychev, V. M. Shalaev and A. Wei, *Nano Lett.*, 2004, **4**, 153–158.

36 K. L. Wustholz, A. I. Henry, J. M. McMahon, R. G. Freeman, N. Valley, M. E. Piotti, M. J. Natan, G. C. Schatz and R. P. Van Duyne, *J. Am. Chem. Soc.*, 2010, **132**, 10903–10910.

37 I. García, A. Sánchez-Iglesias, M. Henriksen-Lacey, M. Grzelczak, S. Penadés and L. M. Liz-Marzán, *J. Am. Chem. Soc.*, 2015, **137**, 3686–3692.

38 C. E. Talley, L. Jusinski, C. W. Hollars, S. M. Lane and T. Huser, *Anal. Chem.*, 2004, **76**, 7064–7068.

39 G. Wang, J. D. Driskell, M. D. Porter and R. J. Lipert, *Anal. Chem.*, 2009, **81**, 6175–6185.

40 K. Kneipp, M. Moskovits and H. Kneipp, *Surface-enhanced raman scattering physics and applications*, 2006, vol. 103.

41 I. Camby, M. Le Mercier, F. Lefranc and R. Kiss, *Glycobiology*, 2006, **16**,137R-157R.

42 M. Cho and R. D. Cummings, *J. Biol. Chem.*, 1995, **270**, 5207–5212.

43 L. Guerrini, F. McKenzie, A. W. Wark, K. Faulds and D. Graham, *Chem. Sci.*, 2012, **3**, 2262-2269.

44 F. S. Ameer, W. Hu, S. M. Ansar, K. Siriwardana, W. E. Collier, S. Zou and D. Zhang, *J. Phys. Chem. C*, 2013, **117**, 3483–3488.

45 B. L. Darby and E. C. Le Ru, *J. Am. Chem. Soc.*, 2014, **136**, 10965–10973.

46 F. Bellutti Enders, F. van Wijk, R. Scholman, M. Hofer, B. J. Prakken, A. van Royen-Kerkhof and W. de Jager, *Arthritis Rheumatol.*, 2014, **66**, 2281–2289.

47 K. T. Liu, Y. H. Liu, Y. H. Chen, C. Y. Lin, C. H. Huang, M. C. Yen and P. L. Kuo, *Int. J. Mol. Sci.*, 2016, **17**, 832.

48 Á. G. Barrientos, J. M. De la Fuente, T. C. Rojas, A. Fernández and S. Penadés, *Chem. - A Eur. J.*, 2003, **9**, 1909–1921.

49 N. G. Bastús, J. Comenge and V. Puntes, *Langmuir*, 2011, **27**, 11098–11105.

